
Latent Beam Diffusion Models for Decoding Image Sequences

Guilherme Fernandes¹, Vasco Ramos¹, Regev Cohen², Idan Szpektor², Joao Magalhaes¹

¹NOVA LINCS, NOVA School of Science and Technology, Portugal

²Google Research

jmag@fct.unl.pt, szpektor@google.com

Abstract

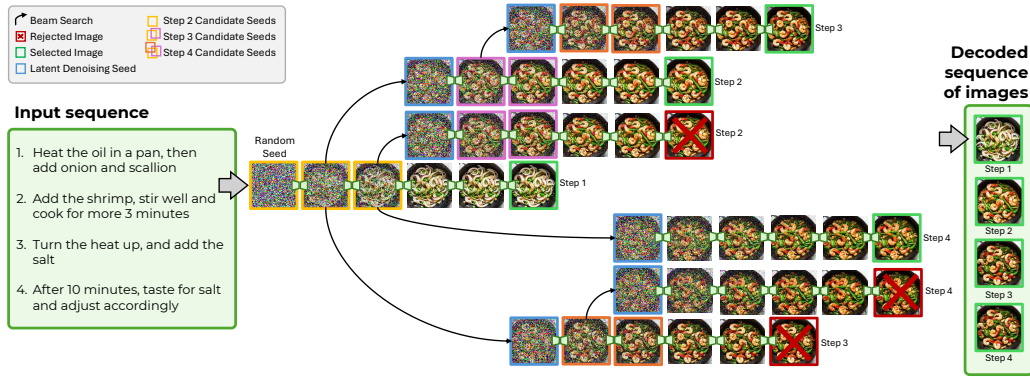
While diffusion models excel at generating high-quality images from text prompts, they struggle with visual consistency in image sequences. Existing methods generate each image independently, leading to disjointed narratives — a challenge further exacerbated in non-linear storytelling, where scenes must connect beyond adjacent frames. We introduce a novel beam search strategy for latent space exploration, enabling conditional generation of full image sequences with beam search decoding. Unlike prior approaches that use fixed latent priors, our method dynamically searches for an optimal sequence of latent representations, ensuring coherent visual transitions. As the latent denoising space is explored, the beam search graph is pruned with a cross-attention mechanism that efficiently scores search paths, prioritizing alignment with both textual prompts and visual context. Human and automatic evaluations confirm that BeamDiffusion outperforms other baseline methods, producing full sequences with superior coherence, visual continuity, and textual alignment. All data and code implementations will be released after publication.

1 Introduction

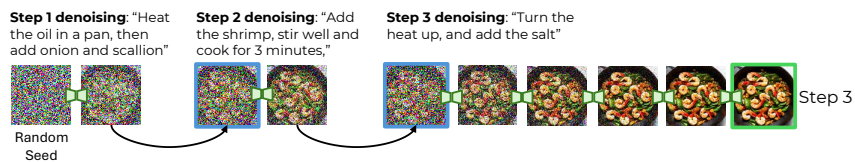
Image diffusion models [43, 9, 44] have made significant advancements in generating high-quality images. These models, especially when combined with text prompts, have shown great potential in producing detailed and contextually accurate visuals [35, 29, 38]. Despite the impressive results at generating individual images based on specific text prompts, diffusion models face challenges when it comes to creating coherent sequences of images. In most cases, each image is generated independently based on its own prompt, which does not naturally ensure visual continuity across a *sequence of correlated prompts*. This problem is further compounded when the narrative is non-linear, where a scene may be connected not only to the immediate prior scene but also to earlier scenes in the sequence. This dynamic can result in sequences that lack coherence and visual consistency over time [2].

We propose to utilize beam search as a potential solution to this problem. Beam search is a well-established technique in text generation tasks like machine translation [14, 51, 17, 37], allowing the model to explore multiple possible paths during the generation process, evaluating different trajectories and refining its predictions. However, despite its success in other domains, it has been barely explored in this context, leaving its potential untapped. In full image sequence generation, beam search could help navigate the complex latent space, refining coherence by adjusting to multiple text prompts or adding semantic cues.

In this work, we explore beam search for latent prior selection in image sequence generation. While previous research has used latent representations as priors to improve sequence consistency [2, 33], it remains unclear which specific representations yield the best overall sequence. We build on these



(a) The beam denoising search tree.



(b) Example of one complete decoded denoising process using contextual captions.

Figure 1: The BeamDiffusion model works in the denoising latent space by denoising the initial seed to latents and them decoding different beam paths. This shows how our method evolves in the latent space and how it can explore the latent space.

ideas by introducing beam search to explore the latent space, enabling iterative refinement of image sequences. As illustrated in Figure 1a, our approach leverages search in the latent space to identify the best sequence of images, minimizing the risk of falling into suboptimal or incoherent paths, while maintaining visual continuity across images. As the beam diffusion algorithm traverses the latent space, the number of hypothesis grow and the least probably search paths are pruned to keep a fixed number of candidate paths. To this end, we incorporate a cross-attention mechanism [19] that evaluates and scores candidate image paths based on their alignment with both the textual description of the next step and the visual context of previous steps. This provides a reliable quality measure for each path, allowing us to retain the best ones while pruning the least suitable, ensuring both adherence to instructions and visual continuity throughout the sequence.

We evaluated the effectiveness of BeamDiffusion in three domains: the Recipes domain and in the out-of-domain DIY and Visual Storytelling. Results obtained with human annotations, automatic evaluations and LLM-as-a-judge, all showed that the proposed approach outperforms baseline methods for generated sequence quality, showcasing its adaptability to diverse contexts.

2 Related Work

Decoding methods are crucial for enhancing the quality of large language models (LLMs). Techniques such as beam search, top-k and nucleus sampling are widely studied for their effectiveness in balancing computational cost with generating coherent, contextually appropriate outputs [40, 10, 7]. Beam search has also proven effective in tasks like machine translation [25], image captioning [48, 15], and visual storytelling [12].

Ensuring coherence remains a major challenge in multimodal sequence generation [8, 22, 4, 16]. Some approaches, like AR-LDM [28], encode the context of caption-image pairs into multimodal representations to maintain consistency across outputs. Likewise, Rahman et al. [32] incorporates the history of U-net [36, 39] latent vectors to preserve narrative coherence. Other approaches, such as Gill [18], combine LLMs with image encoder-decoder systems. StoryDiffusion [52], changes the U-Net’s cross-attention mechanism enabling training-free consistency by sampling tokens from

previous images to maintain coherence in newly generated frames. StoryGen [21] denoises the previous image and the resulting features serve as conditioning for the subsequent generation of images. GenHowTo [45] uses a control net during inference to project the previous image directly into the latent space to guide the diffusion process for the next image step. StackedDiffusion [26] processes stacked image sequences as a single latent representation allowing the attention mechanism to consider all steps together, enhancing coherence across steps. In [2], authors proposed to use latent information from previous steps to guide coherent generation of subsequent images relying on a greedy heuristic-based selection. CoSeD [33] improved on this idea and introduced a contrastive learning approach [3] to rank images generated from different latent seeds. However, both approaches focused on local refinements rather than optimizing throughout the sequence. Our beam search approach extends these local selection criteria to perform global optimization.

While effective for certain tasks, these models suffer from alignment issues, with retrieved or generated images failing to match the narrative context, and they too often require complex training. Our method addresses these previous constraints by generating images directly from the guiding text, maintaining consistency via a beam search for optimal seeds, similar to methods such as [41] that view image generation as a search process.

3 Generating Non-Linear Visual Sequences

Generating a full sequence of visually coherent images from textual scene descriptions is a challenging research problem. Given a sequence of steps $S = \{s_1, s_2, \dots, s_L\}$, where each sequence step s_j is a textual description, our goal is to generate a corresponding sequence of images $\{I_1, I_2, \dots, I_L\}$ that maintain consistency across all steps of the sequence. While Latent Diffusion Models (LDMs) [35] can generate high-quality images in a compressed latent space, this latent space is designed to generate images independently, starting from a randomly initialized latent z_T .

LDMs encode an input image I into the latent space representation z using an encoder \mathcal{E} and reconstruct it through a decoder \mathcal{D} [35]. The reverse diffusion process is modeled by a U-Net backbone [36], ϵ_θ , which incorporates a cross-attention mechanism [47] to condition the denoising iterations on an external input, e.g. the output embeddings of a text encoder $\tau_\theta(s)$. LDMs are trained to iteratively estimate a denoised variant of z , with the loss

$$L_{\text{LDM}} = \mathbb{E}_{\mathcal{E}(I), s, \epsilon \sim \mathcal{N}(0,1), t} [\|\epsilon - \epsilon_\theta(z_t, t, \tau_\theta(s))\|_2^2] \quad (1)$$

This loss evidences the lack of awareness of other denoising processes, making it challenging to ensure consistency across correlated prompts or previous denoising processes. This is particularly challenging in non-linear narratives [42], where maintaining character identity, lighting, and environmental details are crucial. To address these challenges, prior work [32, 21, 45, 2, 33] reuse latent denoising iterations from earlier steps in the sequence, paving the way to a key question: *how to determine the optimal set of denoising latents that maximizes coherence across different generations?* The answer lies in a combinatorial search space, that BeamDiffusion can traverse with a search strategy to determine an optimal solution, as we will discuss next.

3.1 Beam Diffusion Model

To address the limitations of standard LDMs in generating coherent image sequences, we introduce the BeamDiffusion model. The proposed approach aims to enhance both the consistency and quality of image sequences by adopting a strategy inspired by beam search, but with a twist, it operates on latent denoising space. BeamDiffusion incorporates latent representations from previously generated images. These latent representations guide the generation of new candidates, ensuring that each new image aligns with the context of the evolving sequence. This approach allows visual elements from previous images to be carried over or referenced, maintaining contextual consistency and continuity, while also adapting to the next scene description.

In the remainder of this article, the term *step* will always refer to an element in the input sequence; and the term *iteration* will refer to one denoising iteration of the diffusion model.

Algorithm 1 BeamDiffusion Algorithm

```
1: Input parameters:  
    $\{s_1, \dots, s_N\}$ : sequence of steps;  $r$ : number of random seeds;  $m$ : steps back;  $w$ : beam width.  
2:  $\hat{B}_1 \leftarrow \{\text{SD}(s_1, \text{rnd})\}^r$   $\triangleright$  Beam initialization with  $r$  different images.  
3: for  $j = 2$  to  $L$  do  
4:   for all beam  $b \in \hat{B}_{j-1}$  do  
5:      $\mathcal{Z}_j \leftarrow \{\hat{B}_{j-n}, \dots, \hat{B}_{j-1}\}$   $\triangleright$  Read denoising latents from previous steps.  
6:     for all latent  $z \in \mathcal{Z}_j$  do  
7:        $I_j \leftarrow \text{SD}(s_j, z)$   $\triangleright$  Generate candidate a image.  
8:        $\hat{B}_{j-1} \leftarrow \hat{B}_{j-1} \cup I_j$   $\triangleright$  Extend beam with candidate image.  
9:     end for  
10:  end for  
11:   $\text{score}(I_j) \leftarrow \varphi(I_j \in \hat{B}_j)$   $\triangleright$  Score the new image of the beam.  
12:   $B_j \leftarrow \arg \max_{|B_j|=w} \text{score}(\hat{B}_j)$   $\triangleright$  Prune beams and keep top  $w$  beams.  
13: end for  
14: return best beam  $B^* \leftarrow \arg \max_{B_L} \text{score}(B_L)$ 
```

3.1.1 Latent Space Exploration with Diffusion Beams

To generate coherent and diverse image sequences, we explore the latent space of diffusion models using a beam search-inspired strategy. For each sequence step j we generate a set of candidate images $\mathcal{I}_j = \{I_j^{(1)}, I_j^{(2)}, \dots\}$, where each $I_j^{(k)}$ is conditioned on a different beam path.

Sampling the Denoising Latent Space. In our approach, the denoising process for each sequence step is conditioned by representations from prior steps, helping the model maintain coherence across the sequence. In the first step of the sequence, s_1 , we generate multiple candidate images by running the diffusion process with r random noise seeds (Alg. 1, line 2). This strategy enables broader exploration of the latent space and reduces Bayes risk [1], as detailed in Appendix D.

For every generation process corresponding to a sequence step s_i , we store the first N latent space vectors $z_i = \{z_{i,t}\}_{t \in \{1, \dots, N\}}$ produced during the denoising iterations. On each step prompt $s_{j>1}$ we need to generate diverse samples that (a) explore different denoising trajectories in the latent space, and (b) are strongly correlated with previous samples. Leveraging the stored latent space vectors, we sample the latent subspace of n previous denoising processes. Hence, for steps $j > 1$, to enable contextual consistency, we first accumulate representations from the previous m steps:

$$\mathcal{Z}_j = \bigcup_{i \in \{j-m, \dots, j-1\}} \{z_i\}. \quad (2)$$

To generate new candidate images $\mathcal{I}_j = \{I_j^{(1)}, \dots, I_j^{(k)}, \dots, I_j^{(N-m)}\}$ at step j , we condition the diffusion model on the latent trajectories in \mathcal{Z}_j . Specifically, for each latent trajectory $z \in \mathcal{Z}_j$, the model performs a new diffusion process to produce a corresponding image candidate $I_j^{(k)}$, Alg. 1, line 5 and 7. This step establishes a dependency between generations, where latents from earlier steps guide the synthesis of visually coherent transitions over time, as illustrated in Figure 1.

Diffusion Beams. Inspired by beam search [50], which maintains and extends the most promising candidates at each sequence step, we introduce *diffusion beams* to structure sequential image generation. At each step j , the set of candidate images \mathcal{I}_j is used to compute the set of candidate diffusion beams \hat{B}_j : for each step j we consider all the beams existing in step $j - 1$ and extend each one of such b beams $\hat{B}_{j-1}^{(b)}$ by pairing it with a new candidate image $I_j^{(k)} \in \mathcal{I}_j$. The resulting beams are defined as

$$\hat{B}_j = \bigcup_{(b,k)} \left\{ \hat{B}_{j-1}^{(b)} \oplus I_j^{(b \cdot k)} \mid I_j^{(b \cdot k)} \in \mathcal{I}_j \right\}, \quad (3)$$

where \oplus denotes the concatenation of a prior beam with a new candidate image, and $(b \cdot k)$ indexes the pairing of beam b and candidate image $I_j^{(k)}$. This process builds a tree of candidate sequences, Alg. 1, line 8, enabling the model to explore diverse yet coherent visual narratives over time.

3.1.2 Pruning Diffusion Beam Paths

Tracking multiple *diffusion beams* enables BeamDiffusion to maintain visual coherence while exploring diverse continuations across a sequence. However, as the sequence length increases, the number of candidate beams grows rapidly, making it computationally infeasible to retain them all. To address this, we apply a pruning strategy based on a learned contrastive scoring function, which allows us to retain only the most promising beams while preserving diversity.

At each sequence step j , we construct a set of candidate beams \hat{B}_j . Each candidate beam $\hat{B}_j^{(b)}$ is formed by extending a beam from the previous step $\hat{B}_{j-1}^{(b)}$ with a newly generated image $I_j^{(k)}$. A complete candidate beam at step j is a sequence of images $\hat{B}_j^{(b)} = [I_1^{(b)}, I_2^{(b)}, \dots, I_j^{(b)}]$, one per step. To evaluate the overall quality of a beam, we use a contrastive classifier [33], denoted by φ . Specifically, for each image $I_i^{(b)}$ in the beam, the classifier φ computes a compatibility score based on the image’s prompt s_i and the previous images in the beam $B_{i-1}^{(b)}$, which includes earlier images and prompts in the same beam. The total beam score is then the sum of these per-image scores over all sequence steps up to j :

$$\text{score}(\hat{B}_j^{(b)}) = \sum_{i=1}^j \log \left(\frac{\exp(\varphi(I_i^{(b)}, s_i, B_{i-1}^{(b)}))}{\sum_{I'_i \in \mathcal{I}_i} \exp(\varphi(I'_i, s_i, B_{i-1}^{(b)}))} \right), \quad (4)$$

where \mathcal{I}_i is the set of all candidate images at sequence step i . The contrastive formulation ensures that each image is evaluated not in isolation, but relative to other candidates, capturing how well it fits the evolving sequence context.

Once scored, we prune the beam candidates by selecting the top w scoring beams:

$$B_j = \operatorname{argmax}_{B_j \subseteq \hat{B}_j, |B_j|=w} \left(\sum_{i=1}^w \text{score}(\hat{B}_j^{(i)}) \right), \quad (5)$$

where B_j denotes the final set of retained beams for sequence step j .

To balance exploration and efficiency, pruning is disabled for the initial steps, allowing all candidates to be retained initially. After a few step, we apply pruning to keep only the top w beams. This strategy ensures wide exploration early on and focused, high-quality continuation in later sequence steps.

Training. The contrastive classifier $\varphi(I_j | \{s_1, \dots, s_j\}, \{I_1, \dots, I_{j-1}\})$ is trained as a *next image prediction* task to estimate how well align an image is with the previously sequence of steps and images. For a given sequence t and sequence step j , the ground-truth label $l_{t,j}$ indicates whether image I_j belongs to the sequence given its prompt s_j and context $B_{j-1}^{(b)}$. Negative examples are hallucinated from other sequences. The model minimizes the cross-entropy loss encouraging the model to promote candidates that best match the sequence’s semantic and visual dynamics. See appendix A for implementation details.

4 Experimental Setup

In this section, we describe the experimental setup to evaluate BeamDiffusion’s performance in generating coherent image sequences. We outline the datasets used, identify other baseline methods, and explain the human, automatic and LLM-as-a-judge (Gemini [34]) evaluations focused on semantic and visual consistency across generated sequences.

Datasets. We used a dataset consisting of publicly available manual tasks in the Recipes and DIY domains [2], as well as the Visual Storytelling (VIST) dataset [13]. Recipes serve as the in-domain dataset, while DIY tasks and VIST are out-of-domain. These out-of-domain datasets allow us to assess the generalizability of our model across different task domains. More details can be found in Appendix B.2.

Baselines. To evaluate the performance of our image sequence generation method, we compared BeamDiffusion with SD2.1 [35] against two other competing approaches to generate image sequences: GILL [18] and StackedDiffusion [26]. Additionally, we considered two decoding strategies: Greedy

and Nucleus Sampling [11]. As these decoding strategies are novel in the context of image generation, we provide a brief explanation of each. All methods used 50 denoising iterations.

In the Greedy approach, a new image is generated at each step using the first five latents from the previous image, with the image that scores highest overall being selected. Although this is similar to CoSeD_{len=1} [33], it differs in that it relies exclusively on CLIP for selection without any learned module, whereas CoSeD incorporates a trained selection mechanism.

In contrast, Nucleus Sampling introduces diversity by sampling from the subset of images whose cumulative CLIP-assigned probability exceeds a predefined threshold p . Rather than always selecting the most likely image, this method favors high-probability outcomes while allowing for variation in the generated sequence.

Human Evaluation. To find the optimal hyperparameters, the annotators compared pairs of beam search configurations to select the optimal beam width (w in Eq. 5) and steps back (m in Eq. 2). The winning configuration is compared against other configurations until a new configuration is selected as better. The selection criteria focused on semantic alignment and visual consistency. Semantic alignment assesses how well the image sequence matches the corresponding text, while visual consistency evaluates the coherence of the visuals across the sequence (e.g., keeping backgrounds, objects, or ingredients consistent).

Having chosen the optimal configuration, we compared BeamDiffusion to other methods. In the second annotation experiment, BeamDiffusion was compared with other baseline models. Annotators independently assessed the sequences, selecting the best method according to semantic and visual consistency with the possibility of choosing multiple options or none. For further information, see Appendix B.1.

Gemini Evaluation. To further validate our findings and annotate a wider range of tasks, we used Gemini for both evaluation of configurations and baselines. Its selection process closely mirrored that of human annotators. For details, please refer to Appendix B.1.

Human-Gemini Agreement. We conducted an alignment assessment to measure the agreement between human annotators and Gemini. For this, human annotators were asked to rate 16 Recipes, 10 DIYs, and 10 VIST tasks. These ratings were then compared to the evaluations made by Gemini. To quantify the agreement between the two, we computed Fleiss’ kappa [6], obtaining a value of 70%, which indicates a substantial level of agreement. Based on this strong alignment, we extended the evaluation to the remaining sequences using Gemini.

Automatic Metrics. Following prior work [2, 33, 21], we evaluate each method using: (1) *Visual Consistency*, based on average image similarity via DINO [27] (DINO-I) and CLIP [31] (CLIP-I); and (2) *Semantic Alignment*, using CLIP (CLIP-T) to measure similarity between the current image and the average of all step texts up to and including the current one. To place the scores on a comparable scale, we normalize CLIP-I, CLIP-T and DINO by their maximum. Finally, we compute CLIP* as the product between the CLIP-I and CLIP-T, and DINO* as the product between the DINO-I and CLIP-T, this formulations balances visual and semantic quality, while emphasizing semantic alignment, which is critical for accurately reflecting the stepwise input text. See Appendix B.1 for details.

5 Results and Discussion

In this section, we describe the performance of BeamDiffusion based on both human and automatic evaluations. We begin by analyzing the human evaluation, proceed to discussing the automatic evaluations, then focus on specifics of our approach such as hyperparameters and non-linear decoding characteristics, and finally provide a qualitative analysis. Additional statistical information about the results can be found in Appendix B.1.

5.1 General Results

Table 1 compares all methods across three domains: Recipes (in-domain), DIY (out-of-domain), and VIST (out-of-domain). BeamDiffusion consistently outperforms other methods. In the context

Table 1: Frequency of method selection by human annotators(H) and Gemini(G).

Method	Recipes		DIY		VIST	
	H (%)	G (%)	H (%)	G (%)	H (%)	G (%)
GILL [18]	0.0	2.0	0.0	20.0	3.3	16.1
StackedDiffusion [26]	20.0	9.8	12.5	15.6	0.00	3.2
Image Sequence Decoding						
Greedy/CoSeD _{len=1} [33]	0	27.6	0	23.3	0	26.3
Nucleus Sampling [11]	30.0	23.0	37.5	27.7	8.3	26.6
BeamDiffusion	50.0	37.6	50.0	30.0	58.3	34.9

of Recipes, BeamDiffusion is selected 50.0% of the time by humans and 37.6% by the LLM, with Nucleus and Greedy following. In out-of-domain areas, it is chosen once more 50.0% of the time by humans and 30.0% by the LLM-judge for the DIY domain, and 58.3% for humans and 34.9% by the LLM for the VIST dataset. Among sequence generation methods, GILL consistently underperforms across all domains, receiving at most 3.3% of human votes and 16.1% from the LLM in VIST. StackedDiffusion performs better than both Greedy and GILL, but still lags behind BeamDiffusion, with 20.0% of human selections and 9.8% of LLM-judge selections in the Recipes domain.

Overall, BeamDiffusion excels in Recipes and VIST, however performance in DIY remains challenging, with smaller gaps between methods due to the domain’s inherent complexity.

5.2 Automatic Metrics

Table 2 shows that BeamDiffusion achieves the highest CLIP* and DINO* scores (0.40 and 0.30), demonstrating a strong balance between image consistency and semantic alignment. BeamDiffusion excels in maintaining a good compromise between text grounding and image similarity achieving the best result in image consistency (CLIP-I of 0.83 and DINO-I of 0.62). Similarly, for CLIP-T, BeamDiffusion achieves the highest score for image-text alignment (CLIP-T of 0.48). However, in this case, the highest result is shared, as Greedy and Nucleus obtain the same score. This outcome is expected because Greedy and Nucleus utilize CLIP-T to select their outputs by aligning the generated sequence with the text. In terms of sequence generation methods, StackedDiffusion performs better than GILL in all metrics but still lags behind BeamDiffusion and the other decoding methods.

Table 2: Comparison of CLIP-I, DINO-I and CLIP-T across different methods

Method	CLIP-I	DINO-I	CLIP-T	CLIP*	DINO*
GILL	0.55	0.49	0.43	0.23	0.21
StackedDiffusion	0.76	0.46	0.47	0.36	0.22
Image Sequence Decoding					
Greedy	0.81	0.54	0.48	0.39	0.26
Nucleus	0.77	0.53	0.48	0.37	0.25
BeamDiffusion	0.83	0.62	0.48	0.40	0.30

5.3 Best Beam Search Configuration

The hyperparameters beam width (w in Eq. 5) and steps back (m in Eq. 2), play a crucial role in the performance of BeamDiffusion. In this section, we report an exhaustive evaluation on how different beam widths (2, 3, 4, and 6) and steps back (2, 3, and 4) improve the latent selection and the overall quality of the generation. A more detailed discussion on the impact of the latents selection is provided in Appendix C.

We first perform human annotations on a set of sequences to identify the optimal beam search configuration, see Appendix B.1 for details. To determine the best configuration, annotations were used to discard non-optimal configurations. The results in Table 3 showed that the best performing configuration was 2 steps back with a beam width of 4, achieving a selection rate of 25%. Other

Table 3: Influence of different hyperparameter values according to human annotations.

Steps Back	Beam Width			
	2	3	4	6
2	8.33	8.33	25.00	8.33
3	<u>16.67</u>	-	-	-
4	<u>16.67</u>	8.33	8.33	-

Table 4: Influence of different hyperparameter values according to Gemini annotations.

Steps Back	Beam Width			
	2	3	4	6
2	5.71	2.86	48.57	5.71
3	<u>28.57</u>	-	2.86	-
4	-	-	2.86	-

configurations, such as 3 steps back with a beam width of 2 and 4 steps back with a beam width of 2, also showed a strong performance (16.67%), but none outperformed the 2 steps back and beam width of 4 configuration. The configurations with beam width 6 performed the worst in all the settings tested.

To assess the reliability of these findings, we used Gemini for the same evaluation on six tasks, achieving an 85% Fleiss’ Kappa agreement [6], indicating near-perfect alignment. The results from the extended Gemini evaluation (Table 4) confirmed that the optimal configuration, 2 steps back with a beam width of 4, remained the best, now achieving a 48.57% selection rate, a significant improvement over the 33.33% from the initial six-task evaluation. Further, the configuration with 3 steps back and a beam width of 2 still performed well, yielding a 28.57% selection rate, confirming its robustness as an alternative. However, larger beam widths, such as beam width 6, continued to underperform, reinforcing that, in this task, a higher beam width does not always improve performance.

5.4 Non-Linear Sequence Denoising

To analyze how BeamDiffusion explores the latent space, we measured the number of times that a sequence step provides latents for the generation of subsequent steps of the sequence. In this experiment we consider sequences of four steps, (Figure 2). Appendix C.2 provides an analysis at the level of the denoising iterations. Latents from step 1 were chosen 69.9% of the times they had a chance of being selected, highlighting the role of step 1 in shaping the sequence. Selection rates decrease for later steps, with Step 3 at 46.8% and Step 2 at 33.3%. Earlier steps, such as Step 1, have more chances of being chosen, leading to a higher selection rate. Thus, the percentages reflect how often each step is selected given the different possibilities for their inclusion, rather than a simple additive total. This pattern demonstrates how beam search prioritizes crucial steps, particularly Step 1, to establish sequence coherence while strategically weighing intermediate sequence steps.

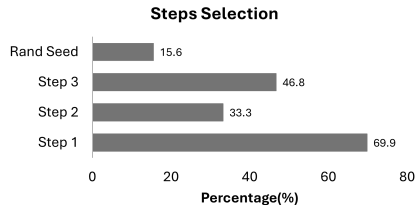


Figure 2: Non-linear steps selection, according to selection opportunities.

5.5 Qualitative Analysis

To highlight how different decoding methods and models impact the semantic and visual consistency of generated outputs, we present several examples in Figures 3a–3c and Appendix F.2. We compare three decoding methods (Greedy, Nucleus, and Beam) with two models (GILL and StackedDiffusion).

In Figure 3a, BeamDiffusion consistently maintains the same pan across all steps, a feature not always seen in Greedy or Nucleus methods. While GILL struggles to follow the step text and results in more inconsistencies, Beam performs better in preserving visual coherence compared to Greedy and Nucleus, though it still faces some challenges. For DIY tasks, as shown in Figure 3b, BeamDiffusion can preserve basic elements such as the color of the plywood and a basic adherence to the text. However, overall, all methods face challenges in capturing precise details. In the VIST dataset, Figure 3c, Greedy and Nucleus alternate between black-and-white and color images, while BeamDiffusion ensures color consistency throughout the sequence. Furthermore, background elements, such as bushes, are maintained in the first three steps, and the individuals in the first and third steps closely resemble each other. Overall, BeamDiffusion excels in maintaining both semantic and visual consistency, even in complex out-of-domain tasks. In contrast, methods such as StackedDiffusion and GILL encounter challenges in keeping a balance between text alignment and consistency across images.

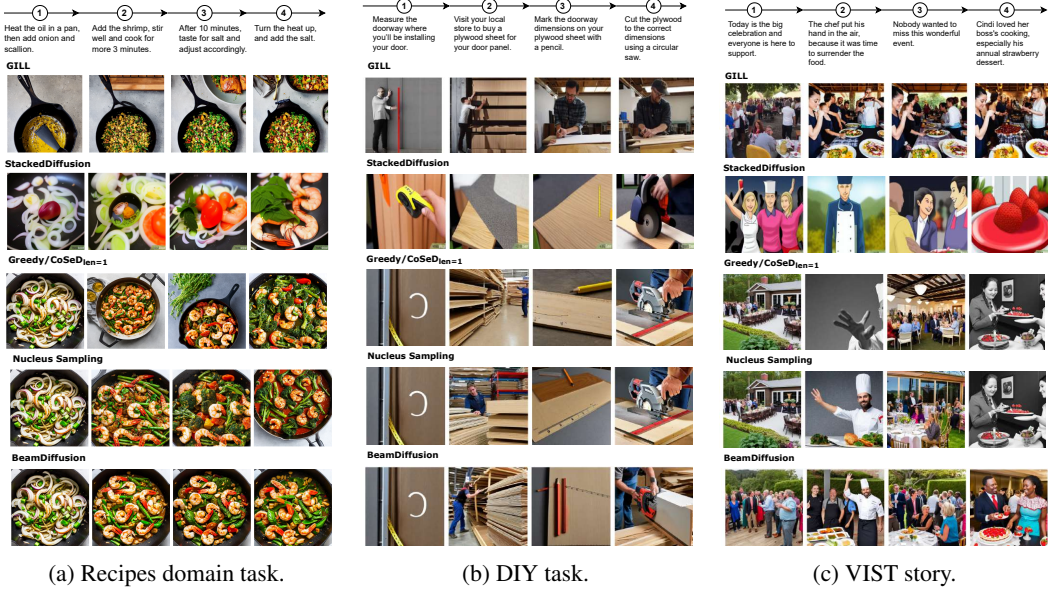


Figure 3: Example tasks from three different domains: Recipes ("Jamaican Callaloo With Shrimp"), DIY ("How to Make a Door"), and VIST ("July 4th Barbecue").

6 Limitations

Exploring the latent denoising space with BeamDiffusion requires Diffusion Models that provide access to fine-grain latents across denoising iterations, where BeamDiffusion still has the opportunity to steer the reverse diffusion process.

The theoretical complexity of BeamDiffusion is linear with the number of beams that we configure the model to explore. The drawback of this strategy is that exploring the space of hypothesis increases the computational complexity of the process. However, this provides a solid ground to explore exciting new ideas where stronger constraints can be enforced in the explored beams.

7 Conclusions

In this paper, we proposed a novel method to explore the latent diffusion space with a beam search strategy, to generate image sequences. BeamDiffusion is a theoretically sound framework, drawing on the strengths of text-based decoding techniques [40], with clear experimental gains over alternative methods, as we demonstrated in generating image sequences with enhanced coherence and consistency.

Through both human and automatic evaluation, we show that beam search performs effectively in generating high-quality and coherent image sequences. The insights drawn from these evaluations reveal that beam search aligns closely with textual instructions while ensuring visual continuity. Most methods can align images with text, however, we demonstrated that *sequence decoding methods perform naturally better at aligning their output with the input sequence*, and BeamDiffusion in particular achieves an optimal balance between the sequence of text instructions and the visual coherence of the generated images. Furthermore, our results underscore the significance of the non-linear selection process in beam search, highlighting how prioritizing certain steps and latents can optimize the quality of the generation process.

This work shows that the latent diffusion space can be steered, offering more reliable and factual outputs. As future work, we plan to explore constraint decoding method that assess the likelihood of each denoise latent with respect to the target prompt. Solving this challenge, will improve the correlation between all elements in a sequence of scenes.

References

- [1] Amanda Bertsch, Alex Xie, Graham Neubig, and Matthew R. Gormley. It’s MBR all the way down: Modern generation techniques through the lens of minimum bayes risk. *CoRR*, abs/2310.01387, 2023.
- [2] João Bordalo, Vasco Ramos, Rodrigo Valerio, Diogo Glória-Silva, Yonatan Bitton, Michal Yarom, Idan Szpektor, and João Magalhães. Generating coherent sequences of visual illustrations for real-world manual tasks. pages 12777–12797, 2024.
- [3] Ting Chen, Simon Kornblith, Mohammad Norouzi, and Geoffrey Hinton. A simple framework for contrastive learning of visual representations. In *International conference on machine learning*, pages 1597–1607. PMLR, 2020.
- [4] Weifeng Chen, Jiacheng Zhang, Jie Wu, Hefeng Wu, Xuefeng Xiao, and Liang Lin. Id-aligner: Enhancing identity-preserving text-to-image generation with reward feedback learning. *arXiv preprint arXiv:2404.15449*, 2024.
- [5] Shaurya Dewan, Rushikesh Zawar, Prakanshul Saxena, Yingshan Chang, Andrew Luo, and Yonatan Bisk. Diffusionpid: Interpreting diffusion via partial information decomposition. *CoRR*, abs/2406.05191, 2024.
- [6] Joseph Fleiss. Measuring nominal scale agreement among many raters. *Psychological Bulletin*, 76:378–, 1971.
- [7] Shaz Furniturewala, Kokil Jaidka, and Yashvardhan Sharma. Impact of decoding methods on human alignment of conversational llms. In *Proceedings of the 14th Workshop on Computational Approaches to Subjectivity, Sentiment, & Social Media Analysis, WASSA 2024, Bangkok, Thailand, August 15, 2024*, pages 273–279. Association for Computational Linguistics, 2024.
- [8] Michal Geyer, Omer Bar-Tal, Shai Bagon, and Tali Dekel. Tokenflow: Consistent diffusion features for consistent video editing. In *The Twelfth International Conference on Learning Representations, ICLR 2024, Vienna, Austria, May 7-11, 2024*. OpenReview.net, 2024.
- [9] Jonathan Ho, Ajay Jain, and Pieter Abbeel. Denoising diffusion probabilistic models. In *Advances in Neural Information Processing Systems 33: Annual Conference on Neural Information Processing Systems 2020, NeurIPS 2020, December 6-12, 2020, virtual*, 2020.
- [10] Ari Holtzman, Jan Buys, Li Du, Maxwell Forbes, and Yejin Choi. The curious case of neural text degeneration. In *8th International Conference on Learning Representations, ICLR 2020, Addis Ababa, Ethiopia, April 26-30, 2020*. OpenReview.net, 2020.
- [11] Ari Holtzman, Jan Buys, Li Du, Maxwell Forbes, and Yejin Choi. The curious case of neural text degeneration. In *International Conference on Learning Representations*, 2020.
- [12] Chao-Chun Hsu, Szu-Min Chen, Ming-Hsun Hsieh, and Lun-Wei Ku. Using inter-sentence diverse beam search to reduce redundancy in visual storytelling. *arXiv preprint arXiv:1805.11867*, 2018.
- [13] Ting-Hao K. Huang, Francis Ferraro, Nasrin Mostafazadeh, Ishan Misra, Jacob Devlin, Aishwarya Agrawal, Ross Girshick, Xiaodong He, Pushmeet Kohli, Dhruv Batra, et al. Visual storytelling. In *15th Annual Conference of the North American Chapter of the Association for Computational Linguistics (NAACL 2016)*, 2016.
- [14] Jungo Kasai, Keisuke Sakaguchi, Ronan Le Bras, Dragomir Radev, Yejin Choi, and Noah A Smith. A call for clarity in beam search: How it works and when it stops. In *Proceedings of the 2024 Joint International Conference on Computational Linguistics, Language Resources and Evaluation (LREC-COLING 2024)*, pages 77–90, 2024.
- [15] Lei Ke, Wenjie Pei, Ruiyu Li, Xiaoyong Shen, and Yu-Wing Tai. Reflective decoding network for image captioning. In *Proceedings of the IEEE/CVF international conference on computer vision*, pages 8888–8897, 2019.
- [16] Levon Khachatryan, Andranik Movsisyan, Vahram Tadevosyan, Roberto Henschel, Zhangyang Wang, Shant Navasardyan, and Humphrey Shi. Text2video-zero: Text-to-image diffusion models are zero-shot video generators. In *Proceedings of the IEEE/CVF International Conference on Computer Vision*, pages 15954–15964, 2023.
- [17] Philipp Koehn and Rebecca Knowles. Six challenges for neural machine translation. In *Proceedings of the First Workshop on Neural Machine Translation, NMT@ACL 2017, Vancouver, Canada, August 4, 2017*, pages 28–39. Association for Computational Linguistics, 2017.

- [18] Jing Yu Koh, Daniel Fried, and Russ Salakhutdinov. Generating images with multimodal language models. In *Advances in Neural Information Processing Systems 36: Annual Conference on Neural Information Processing Systems 2023, NeurIPS 2023, New Orleans, LA, USA, December 10 - 16, 2023*, 2023.
- [19] Hezheng Lin, Xing Cheng, Xiangyu Wu, and Dong Shen. Cat: Cross attention in vision transformer. In *2022 IEEE international conference on multimedia and expo (ICME)*, pages 1–6. IEEE, 2022.
- [20] Shaobo Lin, Kun Wang, Xingyu Zeng, and Rui Zhao. Explore the power of synthetic data on few-shot object detection. In *IEEE/CVF Conference on Computer Vision and Pattern Recognition, CVPR 2023 - Workshops, Vancouver, BC, Canada, June 17-24, 2023*, pages 638–647. IEEE, 2023.
- [21] Chang Liu, Haoning Wu, Yujie Zhong, Xiaoyun Zhang, Yanfeng Wang, and Weidi Xie. Intelligent grimm - open-ended visual storytelling via latent diffusion models. In *CVPR*, 2024.
- [22] Yuan Liu, Cheng Lin, Zijiao Zeng, Xiaoxiao Long, Lingjie Liu, Taku Komura, and Wenping Wang. Syncdreamer: Generating multiview-consistent images from a single-view image. 2024.
- [23] Yujie Lu, Pan Lu, Zhiyu Chen, Wanrong Zhu, Xin Wang, and William Yang Wang. Multimodal procedural planning via dual text-image prompting. In *Findings of the Association for Computational Linguistics: EMNLP 2024, Miami, Florida, USA, November 12-16, 2024*, pages 10931–10954. Association for Computational Linguistics, 2024.
- [24] Richard E. Mayer. Multimedia learning. pages 85–139. Academic Press, 2002.
- [25] Clara Meister, Gian Wiher, and Ryan Cotterell. On decoding strategies for neural text generators. *Trans. Assoc. Comput. Linguistics*, 10:997–1012, 2022.
- [26] Sachit Menon, Ishan Misra, and Rohit Girdhar. Generating illustrated instructions. In *CVPR*, 2024.
- [27] Maxime Oquab, Timothée Darcet, Théo Moutakanni, Huy V. Vo, Marc Szafraniec, Vasil Khalidov, Pierre Fernandez, Daniel Haziza, Francisco Massa, Alaaeldin El-Nouby, Mido Assran, Nicolas Ballas, Wojciech Galuba, Russell Howes, Po-Yao Huang, Shang-Wen Li, Ishan Misra, Michael Rabbat, Vasu Sharma, Gabriel Synnaeve, Hu Xu, Hervé Jégou, Julien Mairal, Patrick Labatut, Armand Joulin, and Piotr Bojanowski. Dinov2: Learning robust visual features without supervision. *Trans. Mach. Learn. Res.*, 2024, 2024.
- [28] Xichen Pan, Pengda Qin, Yuhong Li, Hui Xue, and Wenhui Chen. Synthesizing coherent story with autoregressive latent diffusion models. In *Proceedings of the IEEE/CVF Winter Conference on Applications of Computer Vision*, pages 2920–2930, 2024.
- [29] Dustin Podell, Zion English, Kyle Lacey, Andreas Blattmann, Tim Dockhorn, Jonas Müller, Joe Penna, and Robin Rombach. SDXL: improving latent diffusion models for high-resolution image synthesis. 2024.
- [30] Jordi Pont-Tuset, Jasper Uijlings, Soravit Changpinyo, Radu Soricut, and Vittorio Ferrari. Connecting vision and language with localized narratives. In *Computer Vision–ECCV 2020: 16th European Conference, Glasgow, UK, August 23–28, 2020, Proceedings, Part V 16*, pages 647–664. Springer, 2020.
- [31] Alec Radford, Jong Wook Kim, Chris Hallacy, Aditya Ramesh, Gabriel Goh, Sandhini Agarwal, Girish Sastry, Amanda Askell, Pamela Mishkin, Jack Clark, et al. Learning transferable visual models from natural language supervision. In *International conference on machine learning*, pages 8748–8763. PMLR, 2021.
- [32] Tanzila Rahman, Hsin-Ying Lee, Jian Ren, Sergey Tulyakov, Shweta Mahajan, and Leonid Sigal. Make-a-story: Visual memory conditioned consistent story generation. In *Proceedings of the IEEE/CVF Conference on Computer Vision and Pattern Recognition*, pages 2493–2502, 2023.
- [33] Vasco Ramos, Yonatan Bitton, Michal Yarom, Idan Szepkator, and Joao Magalhaes. Contrastive sequential-diffusion learning: Non-linear and multi-scene instructional video synthesis. In *2025 IEEE/CVF Winter Conference on Applications of Computer Vision (WACV)*, pages 4645–4654, 2025.
- [34] Machel Reid, Nikolay Savinov, Denis Teplyashin, Dmitry Lepikhin, Timothy P. Lillicrap, Jean-Baptiste Alayrac, Radu Soricut, Angeliki Lazaridou, Orhan Firat, Julian Schrittwieser, Ioannis Antonoglou, Rohan Anil, Sebastian Borgeaud, Andrew M. Dai, Katie Millican, Ethan Dyer, Mia Glaese, Thibault Sottiaux, Benjamin Lee, Fabio Viola, Malcolm Reynolds, Yuanzhong Xu, James Molloy, Jilin Chen, Michael Isard, Paul Barham, Tom Hennigan, Ross McIlroy, Melvin Johnson, Johan Schalkwyk, Eli Collins, Eliza Rutherford, Erica Moreira, Kareem Ayoub, Megha Goel, Clemens Meyer, Gregory Thornton, Zhen Yang, Henryk Michalewski, Zaheer Abbas, Nathan Schucher, Ankesh Anand, Richard Ives, James Keeling, Karel Lenc, Salem Haykal, Siamak Shakeri, Pranav Shyam, Aakanksha Chowdhery, Roman Ring, Stephen Spencer, Eren Sezener, and et al. Gemini 1.5: Unlocking multimodal understanding across millions of tokens of context. *CoRR*, abs/2403.05530, 2024.

- [35] Robin Rombach, Andreas Blattmann, Dominik Lorenz, Patrick Esser, and Björn Ommer. High-resolution image synthesis with latent diffusion models. In *Proceedings of the IEEE/CVF conference on computer vision and pattern recognition*, pages 10684–10695, 2022.
- [36] Olaf Ronneberger, Philipp Fischer, and Thomas Brox. U-net: Convolutional networks for biomedical image segmentation. In *Medical image computing and computer-assisted intervention–MICCAI 2015: 18th international conference, Munich, Germany, October 5-9, 2015, proceedings, part III 18*, pages 234–241. Springer, 2015.
- [37] Alexander M. Rush, Sumit Chopra, and Jason Weston. A neural attention model for abstractive sentence summarization. In *Proceedings of the 2015 Conference on Empirical Methods in Natural Language Processing, EMNLP 2015, Lisbon, Portugal, September 17-21, 2015*, pages 379–389. The Association for Computational Linguistics, 2015.
- [38] Chitwan Saharia, William Chan, Saurabh Saxena, Lala Li, Jay Whang, Emily L Denton, Kamyar Ghasemipour, Raphael Gontijo Lopes, Burcu Karagol Ayan, Tim Salimans, et al. Photorealistic text-to-image diffusion models with deep language understanding. *Advances in neural information processing systems*, 35:36479–36494, 2022.
- [39] Tim Salimans, Andrej Karpathy, Xi Chen, and Diederik P. Kingma. Pixelcnn++: Improving the pixelcnn with discretized logistic mixture likelihood and other modifications. 2017.
- [40] Chufan Shi, Haoran Yang, Deng Cai, Zhisong Zhang, Yifan Wang, Yujiu Yang, and Wai Lam. A thorough examination of decoding methods in the era of llms. In *Proceedings of the 2024 Conference on Empirical Methods in Natural Language Processing, EMNLP 2024, Miami, FL, USA, November 12-16, 2024*, pages 8601–8629. Association for Computational Linguistics, 2024.
- [41] Raghav Singhal, Zachary Horvitz, Ryan Teehan, Mengye Ren, Zhou Yu, Kathleen McKeown, and Rajesh Ranganath. A general framework for inference-time scaling and steering of diffusion models. *CoRR*, abs/2501.06848, 2025.
- [42] Marko Smilevski, Ilija Lalkovski, and Gjorgji Madjarov. Stories for images-in-sequence by using visual and narrative components. In *ICT Innovations 2018. Engineering and Life Sciences: 10th International Conference, ICT Innovations 2018, Ohrid, Macedonia, September 17–19, 2018, Proceedings 10*, pages 148–159. Springer, 2018.
- [43] Jascha Sohl-Dickstein, Eric Weiss, Niru Maheswaranathan, and Surya Ganguli. Deep unsupervised learning using nonequilibrium thermodynamics. In *International conference on machine learning*, pages 2256–2265. PMLR, 2015.
- [44] Jiaming Song, Chenlin Meng, and Stefano Ermon. Denoising diffusion implicit models. In *9th International Conference on Learning Representations, ICLR 2021, Virtual Event, Austria, May 3-7, 2021*. OpenReview.net, 2021.
- [45] Tomáš Souček, Dima Damen, Michael Wray, Ivan Laptev, and Josef Sivic. Genhowto: Learning to generate actions and state transformations from instructional videos. In *CVPR*, 2024.
- [46] Raphael Tang, Linqing Liu, Akshat Pandey, Zhiying Jiang, Gefei Yang, Karun Kumar, Pontus Stenetorp, Jimmy Lin, and Ferhan Ture. What the DAAM: interpreting stable diffusion using cross attention. In *Proceedings of the 61st Annual Meeting of the Association for Computational Linguistics (Volume 1: Long Papers), ACL 2023, Toronto, Canada, July 9-14, 2023*, pages 5644–5659. Association for Computational Linguistics, 2023.
- [47] Ashish Vaswani, Noam Shazeer, Niki Parmar, Jakob Uszkoreit, Llion Jones, Aidan N. Gomez, Lukasz Kaiser, and Illia Polosukhin. Attention is all you need. In *Advances in Neural Information Processing Systems 30: Annual Conference on Neural Information Processing Systems 2017, December 4-9, 2017, Long Beach, CA, USA*, pages 5998–6008, 2017.
- [48] Ashwin Vijayakumar, Michael Cogswell, Ramprasaath Selvaraju, Qing Sun, Stefan Lee, David Crandall, and Dhruv Batra. Diverse beam search for improved description of complex scenes. In *Proceedings of the AAAI Conference on Artificial Intelligence*, 2018.
- [49] Zhongqi Wang, Jie Zhang, Shiguang Shan, and Xilin Chen. T2ishield: Defending against backdoors on text-to-image diffusion models. In *Computer Vision - ECCV 2024 - 18th European Conference, Milan, Italy, September 29-October 4, 2024, Proceedings, Part LXXXV*, pages 107–124. Springer, 2024.

- [50] Sam Wiseman and Alexander M. Rush. Sequence-to-sequence learning as beam-search optimization. In *Proceedings of the 2016 Conference on Empirical Methods in Natural Language Processing, EMNLP 2016, Austin, Texas, USA, November 1-4, 2016*, pages 1296–1306. The Association for Computational Linguistics, 2016.
- [51] Yonghui Wu, Mike Schuster, Zhifeng Chen, Quoc V. Le, Mohammad Norouzi, Wolfgang Macherey, Maxim Krikun, Yuan Cao, Qin Gao, Klaus Macherey, Jeff Klingner, Apurva Shah, Melvin Johnson, Xiaobing Liu, Lukasz Kaiser, Stephan Gouws, Yoshikiyo Kato, Taku Kudo, Hideto Kazawa, Keith Stevens, George Kurian, Nishant Patil, Wei Wang, Cliff Young, Jason Smith, Jason Riesa, Alex Rudnick, Oriol Vinyals, Greg Corrado, Macduff Hughes, and Jeffrey Dean. Google’s neural machine translation system: Bridging the gap between human and machine translation. *CoRR*, abs/1609.08144, 2016.
- [52] Yupeng Zhou, Daquan Zhou, Ming-Ming Cheng, Jiashi Feng, and Qibin Hou. Storydiffusion: Consistent self-attention for long-range image and video generation. *CoRR*, abs/2405.01434, 2024.

A Implementation Details

Base Model. Our method is implemented on top of Stable Diffusion v2.1 [35], a latent diffusion model for high-quality text-to-image synthesis. We build upon the open-source implementation provided by Stability AI, extending it to support beam-based generation, latent trajectory tracking, and contrastive scoring mechanisms as described in the main text.

Latent Trajectory Reuse. In our approach, maintaining coherence across sequential generations requires access to the intermediate latent representations produced during the generative process. Fortunately, the model pipeline inherently provides the full sequence of latent representations at each generation step. This enables us to easily extract and reuse specific latents as seed for new generations.

Classifier Training. To train the contextual classifier, we employ a sequence-aware training approach that allows the model to capture dependencies between steps in the generation process. The classifier φ takes as input a candidate image I_l , its textual description s_l , and the previous sequence images and the respective step text ($B_{l-1}^{(b)}$). Then the classifier scores I_j based on how well it fits within the evolving trajectory. During training, we use labels $l_{d,l}$ indicating whether I_l is the correct continuation in the sequence for task d and step l . The model is trained to minimize the cross-entropy loss:

$$\operatorname{argmin} \sum_{d=1}^D \sum_{l=1}^L l_{d,l} \cdot \log(\varphi(I_l, s_l, B_{l-1}^{(b)})), \quad (6)$$

This contrastive training encourages the model to assign high scores to contextually appropriate continuations while penalizing incoherent or semantically unrelated ones. As a result, the classifier learns to distinguish subtle differences in step-to-step coherence, both visually and textually.

Hardware. All experiments were ran on NVIDIA A100 GPUs with 40GB of memory.

B Experiments Details

B.1 Metrics and Annotations

Automatic Metrics. In image sequence generation, CLIP similarity scores between visually similar frames often exceed 0.85, even for near-duplicate content. Wang et al. [49] highlight that such high CLIP-I scores can indicate semantic duplication, which poses a challenge when diversity across frames is desired. While CLIP-I and DINO-I are common proxies for semantic similarity, rewarding near-duplicates undermines meaningful visual progression. Conversely, poor alignment between images and their textual prompts is reflected in low CLIP-T scores. Lin et al. [20] address this by clipping CLIP-T values below 0.1, effectively filtering out weak text-image matches.

To balance these factors, we set CLIP-I scores above 0.9 and DINO-I scores above 0.85 to zero, penalizing visual redundancy. Similarly, we zero out CLIP-T scores below 0.1 to discourage poor alignment with the prompt. This clipping strategy encourages the generation of sequences that are both semantically relevant and visually diverse. In Figure 4, we present the automatic metric scores for a sequence across all methods. The results illustrate that very high CLIP-I values can lead to sequences that fail to follow the textual steps accurately, as observed in the case of GILL. Despite achieving strong visual similarity, the sequence diverges from the intended narrative, highlighting a key limitation of relying solely on CLIP-I. This example reinforces the importance of our clipping strategy: without penalizing excessively high CLIP-I values, the generation process may favor near-duplicates over meaningful visual progression, ultimately undermining semantic fidelity to the prompt.

To complement average scores, we analyze the standard deviation (σ) of these metrics (Table 5). A low σ reflects stable, consistent performance between diverse sequences, while a higher σ implies variability in quality or adaptation to task complexity.

GILL exhibits the highest σ in CLIP-I and DINO-I, indicating its semantic similarity varies significantly between tasks, likely due to inconsistent adherence to step instructions. StackedDiffusion’s

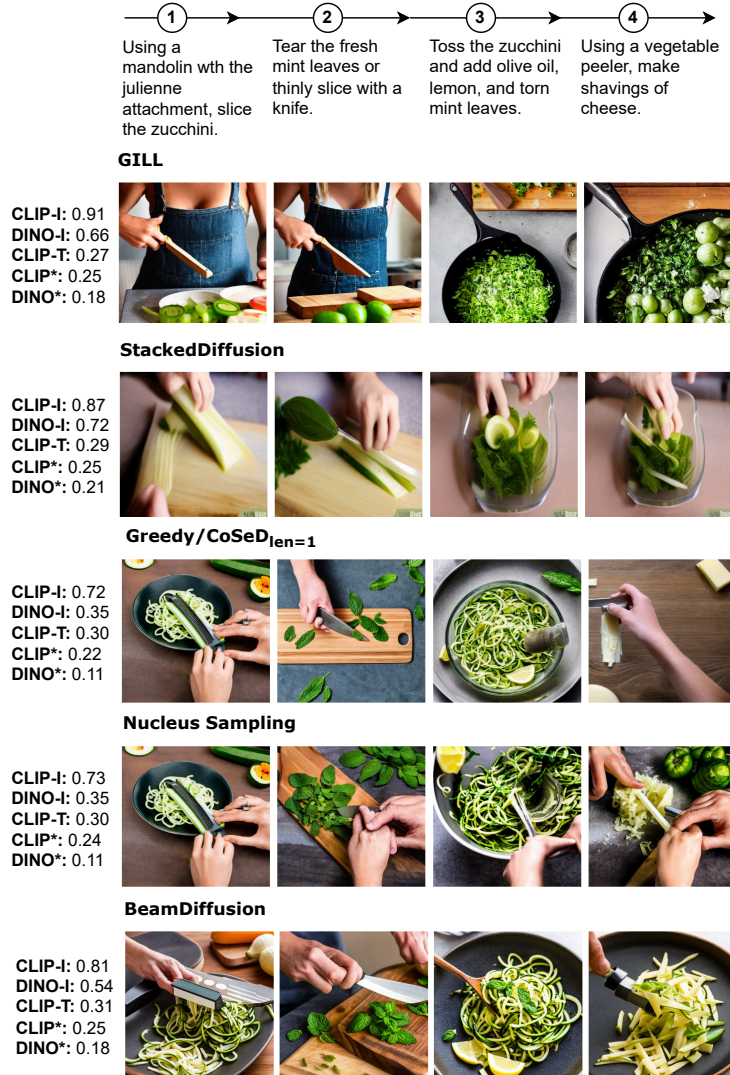


Figure 4: Illustration of the limitation of CLIP-I: despite a high CLIP-I score, the result is not semantically correct or visually faithful. The example compares several automatic metrics (CLIP-T, CLIP-I, DINO-I, CLIP*, DINO*), highlighting discrepancies and failure cases in sequence evaluation.

low σ indicates its consistent performance across different tasks. BeamDiffusion strikes a balance with moderate σ values, indicating a balance between consistency and variation across tasks.

It is worth noting that CLIP-T generally shows lower standard deviation across models, since this metric is explicitly minimized during the diffusion model training. As a result, CLIP-T scores tend to be more stable regardless of the task-specific variation.

Together, the mean and standard deviation metrics suggest BeamDiffusion offers the best combination of high semantic fidelity, text alignment, and stable adaptation across different sequences, making it the most robust method for sequential image generation.

Human annotations. To facilitate the selection of the best beam search configuration, we developed a custom website specifically for human annotation. We found that existing tools lacked the flexibility necessary for our specific use case, especially when evaluating multiple configurations simultaneously. To select the best beam search configuration, 5 annotators are presented with 24 different sequences, each corresponding to a unique beam search configuration.

In total, the 24 configurations were generated by combining three key factors:

Table 5: Comparison of CLIP-I, DINO-I and CLIP-T across different methods with the standard deviation

Method	CLIP-I	DINO-I	CLIP-T
GILL	0.55 ± 0.30	0.49 ± 0.26	0.43 ± 0.08
StackedDiffusion	0.76 ± 0.12	0.46 ± 0.14	0.47 ± 0.09
Image Sequence Decoding			
Greedy	0.81 ± 0.13	0.54 ± 0.14	0.48 ± 0.07
Nucleus	0.77 ± 0.15	0.53 ± 0.15	0.48 ± 0.08
BeamDiffusion	0.83 ± 0.14	0.62 ± 0.18	0.48 ± 0.09

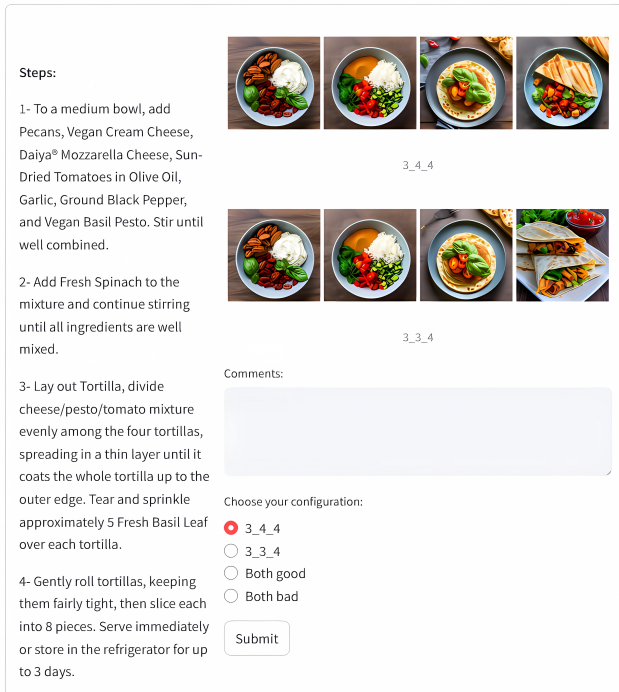


Figure 5: Example of the human annotation elimination round for selecting the best beam search configuration.

- **Steps Back** (m in Eq. 2): This refers to how many previous steps the model uses from its latent representations to explore new candidate outputs. We evaluated three different settings for the number of steps back: 2, 3, and 4, which correspond to using latents from the last two, three, or four images, respectively.
- **Latents Indexes**: We tested two sets of latent configurations, 1, 3, 5, 7 and 0, 1, 2, 3, by selecting specific indexes from the latent representations generated in previous stages. This was done to explore how varying levels of latent detail impact the quality of the generated sequences.
- **Beam Width** (w in Eq. 5): We explored four different beam widths, 2, 3, 4 and 6, which determine how many beams are retained at each step during the search process.

Evaluating all of these at once proved to be exhausting and difficult to manage. To simplify the evaluation process, we adopted an elimination annotation method. In this approach, 5 annotators compare two configurations at a time and select the one with better overall coherence. If neither configuration stands out, annotators can select "both good" or "both bad" (Figure 5), in which case the computationally cheaper option advances to the next round. This process is repeated until we identify the best configuration. This method focuses on direct comparisons, making it easier to pinpoint the most effective beam search settings while also considering computational efficiency.

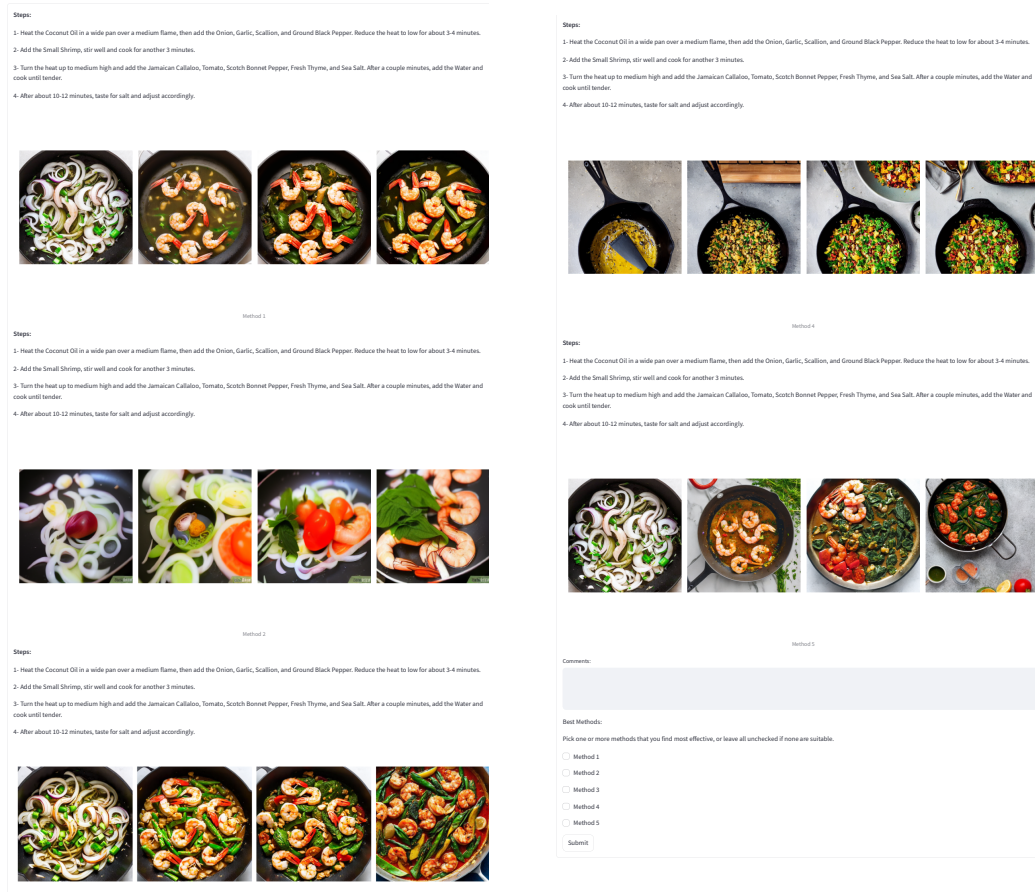


Figure 6: Example of a human annotation to choose the best method.

To evaluate all models performance, annotators are presented with five generated sequences side by side. Figure 6 illustrates an example of this comparison process, where the annotators assess the sequences to determine the most effective approach.

Gemini evaluation. Gemini’s selection process for annotating the best beam search configuration and the best generation method closely mirrored that of human annotators, with one key adjustment: Gemini tends to default to *"both good"* or *"both bad"* when such options are available. To ensure more decisive and accurate results, we removed these options from the prompt. We also refined our comparison methodology. Initially, presenting all five sequences at once led to biased evaluations, as the model disproportionately favored the last two sequences. To mitigate this, we adopted a pairwise evaluation strategy, comparing two sequences at a time. This approach resulted in more balanced and reliable assessments across all comparisons.

Figure 7 shows the prompt used in Gemini to guide the evaluation of image sequences based on visual and semantic consistency.

B.2 Datasets

Recipes and DIYs. Each manual task in both the Recipes and DIYs datasets includes a title, a description, a list of ingredients, resources and tools, and a sequence of step-by-step instructions, which may or may not be illustrated. The Recipes dataset comprises approximately 1,400 tasks, with an average of 4.9 steps per task, totaling 6,860 individual steps. Most tasks feature an image for each step. The DIYs dataset includes a variety of tasks, from simpler projects to more complex ones, with detailed steps.

Gemini Prompt:

"Evaluate two image sequences using the following criteria:

- **Visual Consistency:** Objects, ingredients, backgrounds, colors and styles should remain consistent across frames. Frames should transition smoothly, resembling a video-like progression with no sudden changes or missing elements.
- **Semantic Consistency:** Images must logically follow the described steps, clearly and accurately.

Steps of the process: {steps}

After evaluating all sequences, select the one with the strongest overall consistency (visual and semantic). Pay close attention to even minimal differences, as the sequences are very similar. If both sequences are equally good or bad, choose the one that is slightly better. Choose exactly one of the following options:

- "First sequence"
- "Second sequence" "

Figure 7: Gemini prompt used to select the best beam search configuration and best method.

VIST. We used the Descriptions of Images-in-Isolation (DII) annotations, as they allow for the generation of more precise and informative visual prompts. These annotations provide standalone descriptions of images, making it easier to capture their key visual elements without relying on surrounding context. The dataset includes 50 000 stories, offering a diverse range of visual and textual information. To ensure the most accurate and relevant annotation for each image, we leveraged CLIP. By using CLIP, we were able to select the annotation that best represented the image, improving the quality of our generated prompts and enhancing the overall alignment between text and visuals.

C Impact of Latent Selection on Beam Search Performance

Latent selection plays a crucial role in determining the quality and coherence of image sequences generated through beam search. By analyzing how different latent groups contribute to generation performance, we can better understand their impact on semantic alignment and visual coherence.

This aligns with recent work on interpreting diffusion models. For example, Pont-Tuset et al. [30] ground textual descriptions in image regions, while Tang et al. [46] and Dewan et al. [5] explore how textual prompts influence generation through attention analysis and partial information decomposition. In contrast, our method contributes to interpretability by examining how latent space traversal, guided by beam search, affects the generation of coherent, semantically aligned image sequences.

To systematically investigate this, we evaluate several sequences, each consisting of four steps, allowing us to assess the effects of latent selection across a diverse set of sequences. Using both automatic evaluation and human annotations, we analyze different latent configurations to determine which groups contribute most to generating coherent and semantically meaningful sequences.

C.1 Impact of Latent Groups on Performance

Annotations. Following the initial analysis of beam search configurations (Sec. 5.3), where we used latent indexes 0, 1, 2, and 3, we further investigated the impact of using different latent configurations on the generated sequences. While latents 0, 1, 2, and 3 show promising results, latents 1, 3, 5, and 7 exhibit significantly poorer performance. In particular, beam search configurations for these underperforming latents result in very limited selection rates, indicating they are rarely chosen in both human and Gemini annotations. For human annotations across 6 tasks, the only configuration that yielded any selection was the one with 4 steps back and a beam width of 3, achieving a selection rate of 8.33%. All other configurations resulted in 0% selection. In contrast, none of the configurations showed any non-zero selection rate under Gemini annotations, reinforcing the lack of preference for these latents.

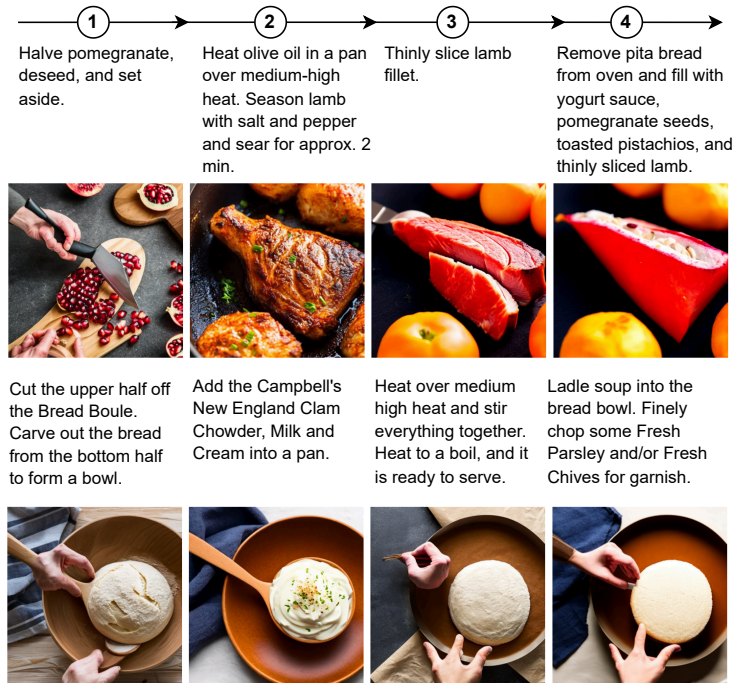


Figure 8: Impact of using 1, 3, 5, and 7 latent configurations on image generation.

Similarly, for Gemini annotations evaluated on the same 6 sequences, the configurations do not yield any notable results, with no selection rates. When the evaluation is extended to 35 sequences, the performance for latents 1, 3, 5, and 7 remains sparse, with a single configuration (2 steps back, beam width of 3) being selected, with a selection rate of 2.86%. Figure 8 visually demonstrates the poor results, where the images appear nearly identical, further supporting the findings of limited diversity and low performance, which aligns with the findings of [33, 2].

Automatic Metrics. Given the observed negative impact of higher latents on performance in human annotations, we investigated how latents influence text-image alignment using the DAAM (Diffusion Attention Attribution Map) framework [46]. DAAM interprets text-to-image diffusion models by analyzing cross-attention maps during the denoising process, generating heat maps that reveal how strongly each prompt token affects different regions of the output image.

By applying DAAM, we examined whether higher latents distort or weaken the influence of key tokens during generation. The resulting heat maps allowed us to visually assess token-level contributions, helping us understand whether the model continues to attend to the most semantically important parts of the prompt under varying latent configurations..

To quantify text alignment, we calculated the average heat map maximum intensity for all tokens, providing a numerical measure of how well the model preserved the key textual elements in the generated image. Then, for each sequence of generated images, we computed the average alignment score across all images in the sequence. While this serves as an objective metric for evaluating text adherence, it remains a partial measure, as it focuses solely on text alignment without accounting for other important aspects of image quality, such as coherence, realism, or artistic fidelity. Figure 9 shows the average impact of different latent groups on text alignment. The results reveal a clear pattern, latents from earlier iterations contribute more effectively to aligning the text with the generated image, while text alignment weakens as we move to higher latent ranges. Specifically, latents in the 0–3 range showed the strongest alignment, with an average score of 1.544, followed by the 4–7 range (1.523). In contrast, latents from the highest index range (16–19) had the weakest influence on alignment, with a significant drop in average scores. This suggests that earlier-stage latents play a crucial role in preserving text fidelity, whereas later-stage latents may dilute or distort the contribution of key tokens.

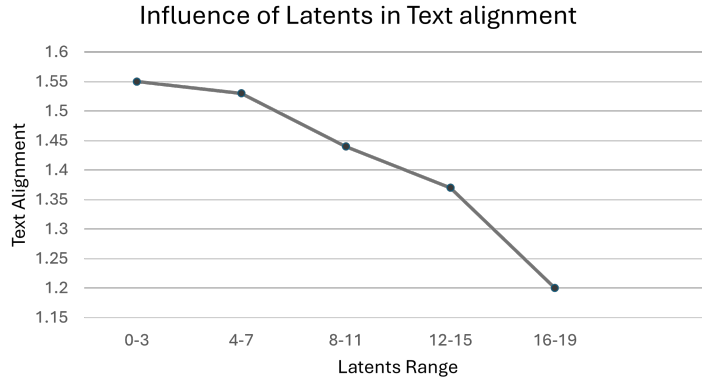


Figure 9: The average influence of latent indices on text alignment across task data.

In Figure 13, we analyze text alignment across multiple steps using heat maps corresponding to different latent groups, revealing how the connection between the input text and the generated image evolves throughout the process. Certain areas, such as the background and the bowl, show little to no heat map activation, indicating that these regions are less influenced by the text and more shaped by the model’s learned priors and overall scene composition. Since the model generates new images by building on latents from previous steps, these early decisions about text relevance persist throughout the process, influencing later refinements. Additionally, when examining generations using later latent groups, we find that this information remains more stable across all steps. This suggests that latents at these stages carry more structural and stylistic details, focusing on consistency rather than continuous adjustments based on the input text.

While later latents are effective at preserving visual consistency from previous steps, they are less capable of incorporating new details from the input prompts. For example, later latent groups (16-19) maintain stability in visual elements throughout the process, preserving previously established features. However, this comes at the expense of adapting to new or changing textual instructions. In contrast, early latent groups (0-3) demonstrate strong alignment between the text and the generated image, with consistently high heat map intensity across all steps. This highlights their role in grounding the image in the input text. For later latent groups (4-7), however, we observe a drop in heat map intensity, particularly by step 3, suggesting the model shifts focus away from strict textual adherence and toward refining finer visual details.

C.2 Latent Selection on Image Sequence Generation

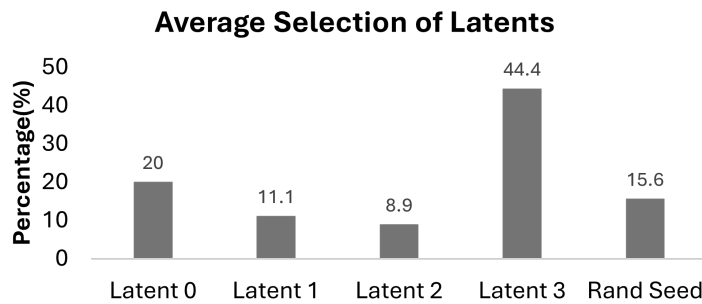


Figure 10: The average number of times that the model selected a given **latent** to generate the next image.

Following our evaluation of the impact of latent groups on performance, we now examine the role of individual latents within the higher-performing group (Latents 0-3). As shown in Figure 10, Latent 3 is selected most frequently (44.4%), followed by Latent 0 (20%), while Latents 1 and 2 are used less often (11.1% and 8.9%, respectively). This uneven distribution suggests that Latents 0

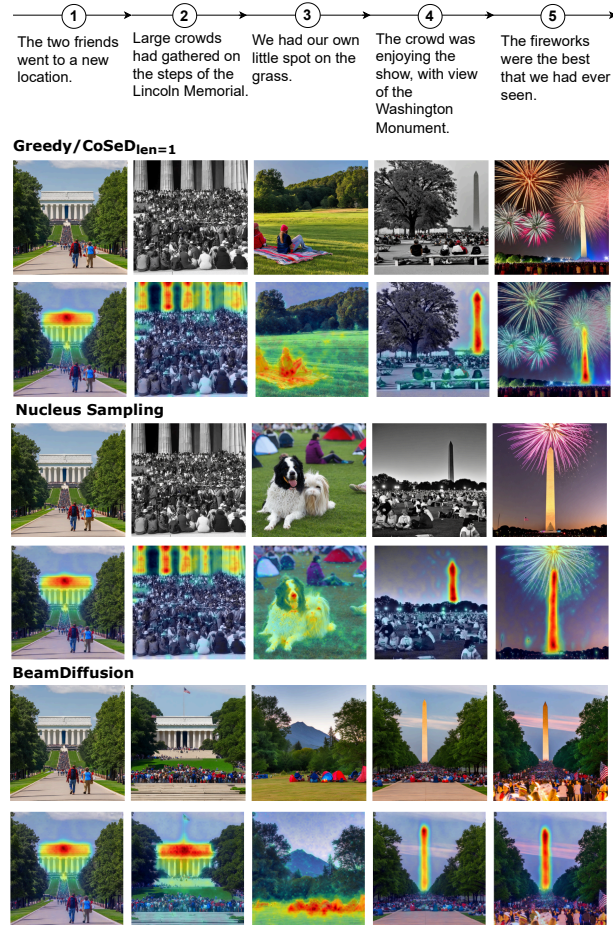


Figure 11: Heat maps illustrating cross-attention in latent diffusion across different decoding methods. The visualizations show variations in how each approach preserves or redistributes attention to textual cues throughout the generation process.

and 3 contribute disproportionately to the generation of sequences with better text alignment. One possible explanation is that these latents encode more semantically relevant or visually discriminative features that align well with the text prompts. Their frequent selection by beam search indicates that these latents are particularly effective at resolving ambiguities or reinforcing important visual cues during sequence generation. The lower usage of Latents 1 and 2 may reflect their tendency to encode less salient or redundant information, which contributes less to text-conditioned coherence. Interestingly, the Rand seed, which injects stochasticity into the generation process, accounts for 15.6% of selections. This suggests that while beam search primarily exploits strong latents like 0 and 3, it also values diversity. The inclusion of randomized elements allows the search to escape local optima and sample from alternative yet plausible paths, enhancing the robustness of the final sequence.

Figure 11 illustrates how different latent search methods affect text-image alignment. The heat maps show how attention patterns shift depending on the decoding strategy, revealing variations in how well each method preserves focus on key textual cues. Notably, in step 3, BeamDiffusion exhibits superior alignment, maintaining a stronger connection to the prompt and ensuring greater sequence coherence compared to other methods.

While Beam Diffusion generally achieves better visual consistency and stronger text adherence in earlier steps, it slightly underperforms in step 5, failing to capture the "fireworks" mentioned in the prompt. This highlights how even methods with strong overall performance can exhibit localized weaknesses, underscoring the importance of analyzing alignment step by step.

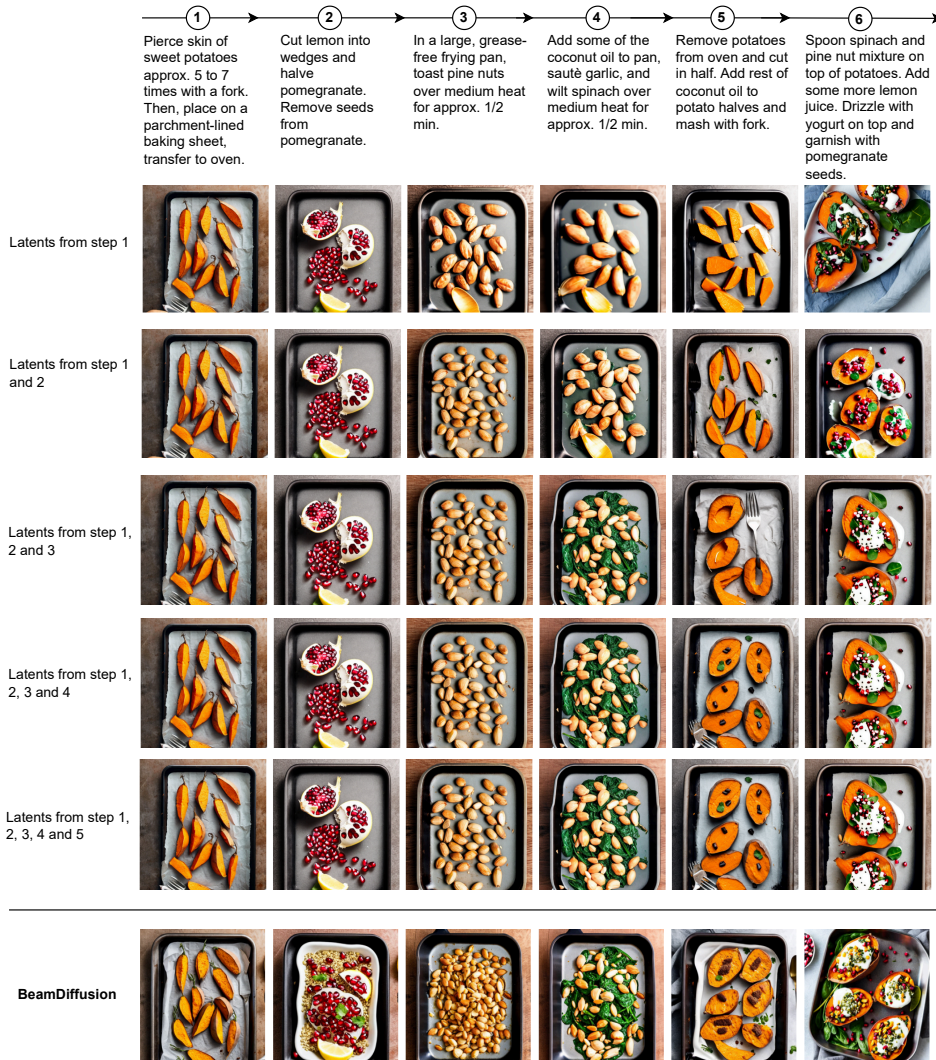


Figure 12: Visual comparison of sequences generated with cumulative latent access. Each row shows a sequence generated using latents from only the first step, the first two steps, and so on, up to all previous steps. The bottom row shows the result from BeamDiffusion, which uses latents from only the two preceding steps.

Overall, these findings highlight the significance of latent selection strategies in optimizing image generation. The results indicate that prioritizing the most significant latents could enhance the coherence of visual sequences and improve text alignment. These observations underline the influence of latent search strategies on the semantic accuracy and coherence of generated outputs.

C.3 Effect of Cumulative Latent Access

To investigate how access to latents from previous steps influences the quality of generation, we conducted an ablation study in which we constrain the set of available latents throughout the generation of the sequence. Specifically, we evaluate performance when the model is limited to latents from only the first step, then from the first two steps, and so on, up to including latents from all previous steps (i.e., full cumulative access).

As shown in Figure 12, limiting the model to latents from only the first step results in weak text-image alignment and incoherent visual transitions. Gradually expanding the latent set to include more steps improves sequence quality, particularly when moving from two to three steps. However, we observe

that including latents from all previous steps does not yield further improvements in coherence, suggesting diminishing returns with increasing temporal access.

In contrast, BeamDiffusion uses latents from only the two most recent steps and achieves results that are comparable, or even superior, to the full cumulative case. This indicates that a narrow temporal window is sufficient to maintain strong alignment and visual consistency. By avoiding the computational cost of considering all previous steps, BeamDiffusion finds a favorable trade-off between quality and efficiency.

Overall, this experiment highlights that cumulative latent access enhances generation quality up to a point, but full historical memory is unnecessary. Strategies such as BeamDiffusion, which take advantage of a limited but informative temporal context, can produce high-quality sequences while significantly reducing computational overhead. These findings also underscore the importance of the non-linear sequence denoising strategy introduced in Section 5.4, which enables more targeted and effective reuse of past latents without the need for full sequence access.

D Minimizing Decoding Risk

The generation process using diffusion models begins with a seed that determines the initial conditions of the model. The choice of this seed significantly affects the outcome, as it influences the path the model takes during generation. Using multiple random seeds in the first step ensures a diverse exploration of possible outputs, avoiding premature narrowing of options into a single path based on that seed. This limits the diversity of the results and increases the chance of missing better options.

Greedy Decoding and Nucleus Sampling. In both greedy decoding and nucleus sampling, we use the same approach in the first step. Multiple random seeds are employed to generate a set of candidate images. Each candidate is then evaluated using the CLIP score mechanism, which compares the generated images with the step text. The image that best aligns with the text, according to the CLIP score, is selected to continue the process. This method ensures that both greedy decoding and nucleus sampling benefit from multiple diverse starting points, increasing the quality and variety of the generated outputs.

BeamDiffusion. In BeamDiffusion, relying on a single random seed in the first step effectively makes the process a greedy selection, as it locks the generation into a specific path. This limits diversity and reduces the chances of discovering higher-quality outputs. By using multiple random seeds, each seed generates a different decoding trajectory, helping to broaden the search space and increasing the likelihood of finding better solutions. Using multiple random seeds in the initial step enhances the exploration of the latent space, ensuring better and more diverse results across different decoding strategies.

Random Seeds for mid-sequence Generation. The sequence of scenes $S = \{s_1, s_2, \dots, s_L\}$ may have one scene in the middle of the sequence that should be independent. To address this, for steps $s_{j>1}$, we use a combination of random seeds and past latent vectors to maintain a balance between diversity and coherence, which is particularly important for such scenarios.

E Broader Impacts and Challenges

In the development and evaluation of the BeamDiffusion method, we encountered several challenges that required careful consideration and innovation. These challenges spanned multiple aspects of the model, ranging from the difficulty of generating accurate and concise captions, to identifying suitable domains for testing, and addressing the computational complexity of the generation process. While we were able to propose solutions for some of these challenges, others remain open and present ongoing areas of research. In this section, we outline the key challenges we faced and the strategies we employed, while acknowledging that not all of them have been fully addressed.

E.1 Impacts

This work proposes a method to improve generative pretraining by incorporating subject-aware mutual information maximization, aiming to produce more contextually aligned and coherent sequences of

images. The ability to generate visually consistent image sequences has positive applications in areas such as animation, visual storytelling, educational media, and accessibility tools (e.g., for generating illustrative content from text). However, as with many generative models, there are potential negative societal impacts. Enhanced coherence and subject fidelity could be misused to create misleading or deceptive visual content, such as more convincing visual disinformation, propaganda, or synthetic media (e.g., deepfakes).

E.2 Contextual Scene Descriptions

One of the challenges encountered concerns the generation of captions that accurately describe the steps involved in the sequence. Often, a single step may consist of multiple sub-steps, each contributing to the overall generation. This makes it difficult to write a single concise caption that captures the full scope of each step. The challenge lies in ensuring that the caption not only reflects the specific action or transformation occurring at each step but also conveys the progression and complexity of the entire sequence. Additionally, if we divide the steps into smaller sub-steps to better describe the process, the sequence becomes very extensive, making it even harder to maintain clarity and readability while ensuring comprehensive coverage of the entire generation process.

To address this challenge, we leverage Gemini [34], specifically the Gemini 1.5 Flash model, to refine step descriptions into visually detailed prompts while considering sequence context. Specifically, Gemini produces a contextualized caption c_j based on the current step description s_j and all preceding steps as follows:

$$c_j = \phi(s_j | \{s_1, s_2, \dots, s_{j-1}\}) \tag{7}$$

Following this approach we can improve image generation prompts by maintaining consistency and preserving the dependencies between sequential steps.

E.3 Domains.

Identifying a domain that effectively highlights the advantages of the BeamDiffusion method, particularly the benefits of beam search, is still a challenge. While BeamDiffusion provides improvements in consistency and coherence, not all domains clearly showcase these advantages. Certain domains may lack the complexity or diversity needed to demonstrate the method’s strengths, such as its adaptive latent selection or its ability to maintain alignment with contextual instructions. Finding a domain that not only aligns with the method’s capabilities but also provides a clear and compelling demonstration of its improvements remains an ongoing challenge.

E.4 Complexity of the generation.

The BeamDiffusion model generates multiple candidate images at each step by exploring a range of latents. We analyze the complexity of the model for a steps back of m steps and N latents explored. In the initial steps, the complexity is high because pruning begins only after the second step. For each beam, $N \cdot m$ latents are explored, and the search space grows exponentially, resulting in significant computational cost in the early stages. During the first two steps, the complexity grows with the number of candidates and latents, proportional to $\mathcal{O}(N \cdot m)^j$ for $j \leq 2$. Specifically, for $j = 1$, the complexity is proportional to the number of explored random seeds. After the second step, pruning reduces the number of candidates to the most promising w beams, decreasing the complexity to $\mathcal{O}(N \cdot m \cdot w)$.

To further reduce complexity, a heuristic based on text relevance can be used to predict the top P most relevant past images. By restricting the search space to the latents of these top P candidates, the model improves efficiency by prioritizing contextually relevant images, particularly in the early steps. While the initial three steps remain computationally demanding due to the expansive search space, pruning combined with this heuristic can significantly lower the computational cost by refining the candidate set.

F Application Examples

This section presents additional visual examples and qualitative results that complement the main paper. Images and other visual aids are essential tools that significantly improve comprehension

across a variety of domains. Whether breaking down complex tasks, illustrating a sequence of events, or clarifying intricate concepts, visual representations provide clear, step-by-step guidance that enhances understanding [24]. From technical procedures and instructional design to storytelling and educational content, multi-scene image sequences help readers grasp information more intuitively, transforming even the most complex or dense topics into something more accessible. However, generating a sequence of images that not only aligns with each textual instruction but also maintains overall coherence remains a major challenge [23]. In this appendix, we include expanded examples to further illustrate how our model addresses this issue. These include additional visualizations of the beam search process and extended qualitative comparisons across domains such as recipes, visual storytelling, and DIY tasks. Together, these examples highlight the strengths and limitations of current approaches in achieving textual alignment and visual consistency in sequential image generation.

F.1 Beam Search Tree

In Figure 14a, we provide another example of how the latent search occurs within the beam denoising process. This illustrates the BeamDiffusion model at work, showing the denoising of the initial seed to latents and how different beam paths are decoded. The figure highlights how our method explores the latent space, iterating through various latents based on the beam search strategy.

In Figure 14b, we observe that the generation of the selected image at step 4 behaves similarly to an isolated diffusion process. However, it is important to note that this process is influenced by multiple prompts. Specifically, the image generation at step 4 is conditioned on the prompts from steps 1, 3, and 4. This demonstrates how the latent search process incorporates context from various steps, showing that even though each generation step seems independent, it is shaped by previous steps, enabling a more coherent and consistent generation of the final image.

F.2 Sequence Examples

To provide a comprehensive comparison between all models, we present several examples across different domains in Figures 15-26. These figures show case how each method performs in terms of maintaining sequence coherence throughout sequential image generation.

In our overall qualitative analysis, we observe that both Greedy/CoSeD_{len=1} and Nucleus Sampling methods are generally good at following the textual input across steps, as shown in Figures 15, 18, 21, and 22. They align well with the step instructions but often struggle with visual consistency, as the generated images show noticeable shifts or inconsistencies between steps. This lack of visual cohesion detracts from the overall coherence of the sequence, even though they adhere reasonably well to the textual prompt. In contrast, GILL and StackedDiffusion exhibit a different behavior. While both maintain high visual consistency, generating sequences in which the images are visually similar, they struggle to accurately follow the step-by-step textual instructions. GILL, in particular, tends to produce images that lack the necessary variability to incorporate new information from each step, resulting in sequences that are visually cohesive but contextually incorrect or incomplete. StackedDiffusion performs slightly better than GILL in this regard, capturing some of the step-wise changes, but still often fails to fully reflect the evolving textual input across the sequence.

Finally, BeamDiffusion strikes a strong balance between text adherence and visual consistency. As shown in Figures 15, 18, 21, and 22, it generally produces the most coherent sequences compared to other methods. In most cases, BeamDiffusion effectively follows the textual instructions while maintaining visual consistency across the steps. This combination of textual alignment and visual stability leads to more coherent and contextually accurate image sequences. While not without its limitations, BeamDiffusion demonstrates a more reliable progression throughout the image generation process than the other approaches. However, it is important to note that all methods face challenges in maintaining coherence within the DIY domain, as seen in Figures 23, 24, and 26. The complexity and diversity of DIY tasks present unique difficulties for the models, making it harder to both accurately follow textual instructions and ensure consistency throughout the sequence. While the models perform well in other domains, the intricacies of the DIY domain result in some inconsistencies, particularly when capturing step changes.

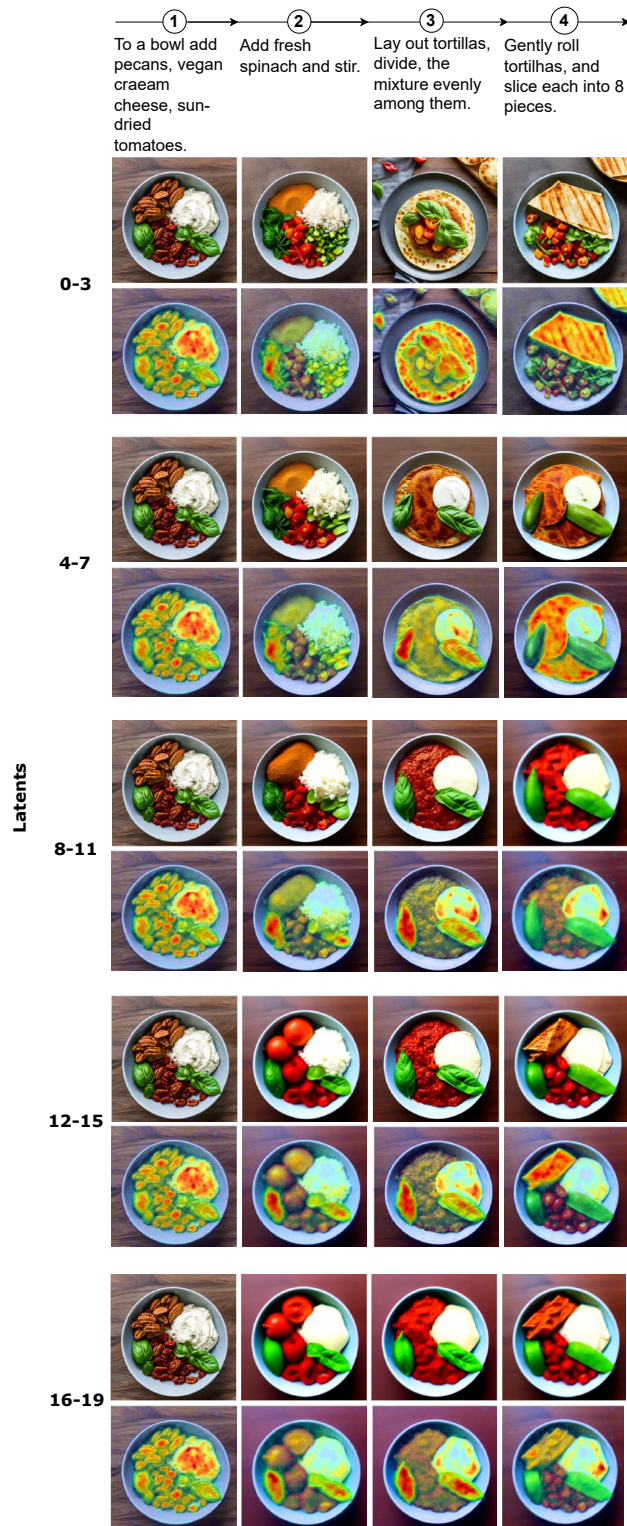
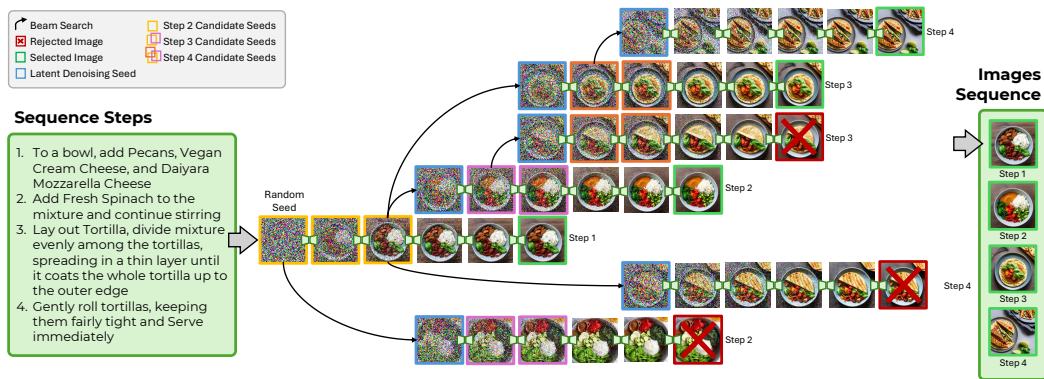
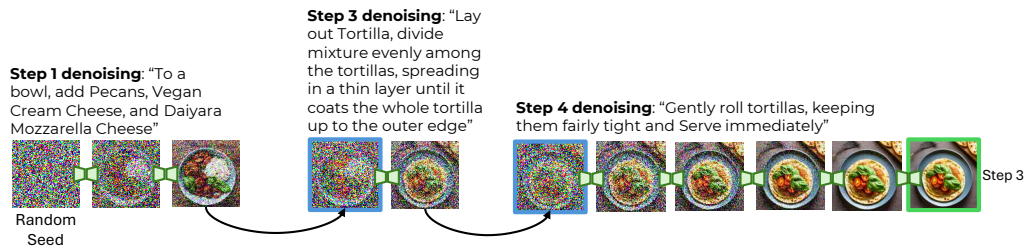


Figure 13: Visualization of cross-attention in latent diffusion across different sets of latents. The heat maps reveal how attention patterns evolve at various sequence steps, highlighting the alignment between text prompts and distinct latent representations.



(a) The beam denoising search tree.



(b) Example of one complete decoded denoising process using contextual captions.

Figure 14: The beam diffusion model works in the denoising latent space by denoising the initial seed to latents and them decoding different beam paths. This shows how our method evolves in the latent space and how it can explore the latent space.



Figure 15: Example of the Recipes domain task "Vegan Basil Pesto and Sun-Dried Tomato Pinwheels", with a sequence of 4 steps.



Figure 17: Example of the Recipes domain task "Zucchini, Pecorino & Mint Salad", with a sequence of 4 steps.



Figure 16: Example of the Recipes domain task "Tangy lemon sheet cake", with a sequence of 4 steps.



Figure 18: Example of the Recipes domain task "Bone Broth", with a sequence of 3 steps.

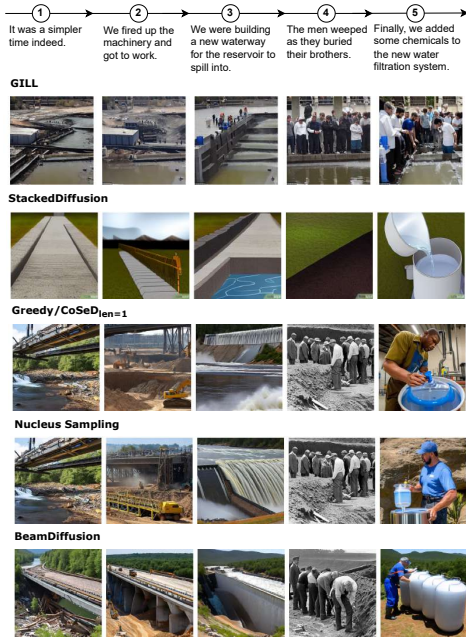


Figure 19: Example of the out-of-domain VIST story "Klamath Project Construction", with a sequence of 5 steps.

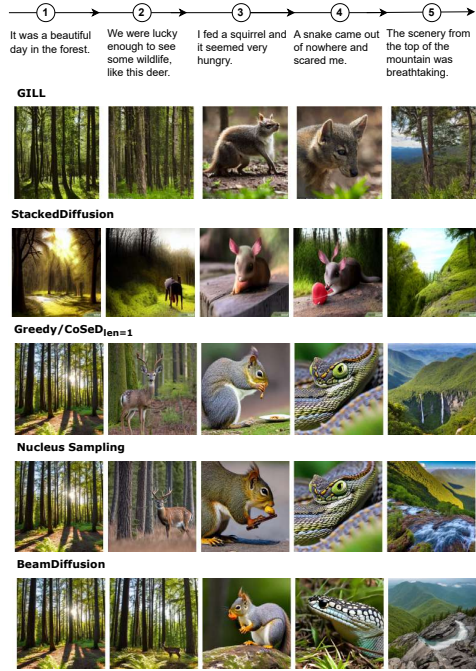


Figure 20: Example of the out-of-domain VIST story "Yosemite Weekend", with a sequence of 5 steps.

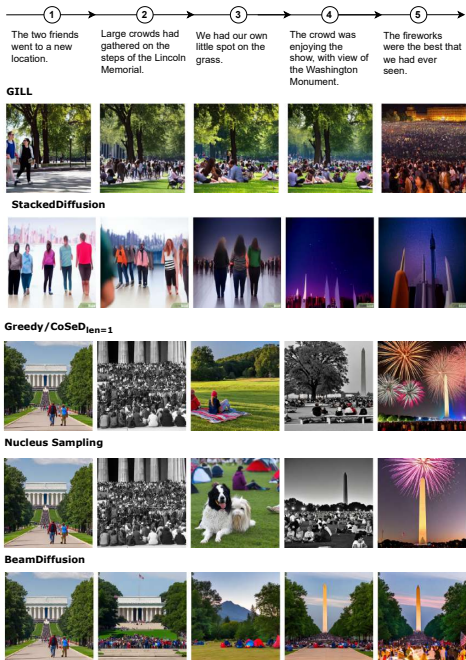


Figure 21: Example of the out-of-domain VIST story "Fireworks - 4th July in Washington, DC", with a sequence of 5 steps.

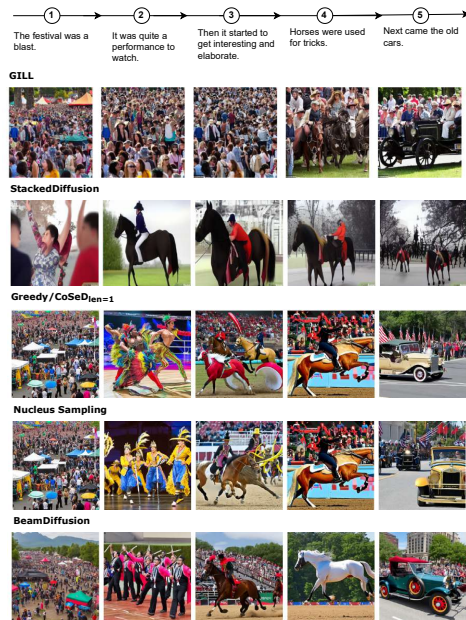


Figure 22: Example of the out-of-domain VIST story "Independence Day Parade", with a sequence of 5 steps.



Figure 23: Example of the out-of-domain DIY task "How to Clean Silk Rugs", with a sequence of 2 steps.



Figure 24: Example of the out-of-domain DIY task "How to Polish Wood", with a sequence of 3 steps.



Figure 25: Example of the out-of-domain DIY task "How to Preserve Basil", with a sequence of 6 steps.

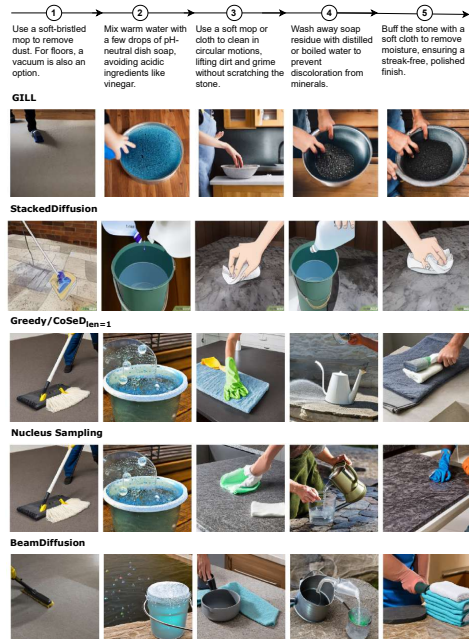


Figure 26: Example of the out-of-domain DIY task "How to Clean Natural Stone", with a sequence of 5 steps.